SCIENTIFIC REPORTS

OPEN

Spectral separation of optical spin based on antisymmetric Fano resonances

Received: 18 August 2015
Accepted: 16 October 2015
Published: 12 November 2015

Xianji Piao, Sunkyu Yu, Jiho Hong & Namkyoo Park

We propose a route to the spectral separation of optical spin angular momentum based on spin-dependent Fano resonances with antisymmetric spectral profiles. By developing a spin-form coupled mode theory for chiral materials, the origin of antisymmetric Fano spectra is clarified in terms of the opposite temporal phase shift for each spin, which is the result of counter-rotating spin eigenvectors. An analytical expression of a spin-density Fano parameter is derived to enable quantitative analysis of the Fano-induced spin separation in the spectral domain. As an application, we demonstrate optical spin switching utilizing the extreme spectral sensitivity of the spin-density reversal. Our result paves a path toward the conservative spectral separation of spins without any need of the magneto-optical effect or circular dichroism, achieving excellent purity in spin density superior to conventional approaches based on circular dichroism.

Optical spin angular momentum (SAM) in relation to the handedness of photons[1] is a topic that has received significant attention. The SAM of light is typically achieved with materials which are distinguishable from their mirror images i.e. optical chiral materials[2–10]. Overcoming the restrictions in natural chiral materials, the field of optical chirality is now entering into a new regime of artificial chirality, with the progress in fabrication technology. Artificially enhanced chiral interactions[4–8,11–13] using sub-wavelength structures have been demonstrated not only for quantum-analogical interactions such as spin-orbit coupling[14,15], but also for a variety of applications, including enantiomer sensing[12,13], negative refraction[16–18], and topological bandgaps[19,20]. Approaches for notable artificial structures also include nature-mimetic 3-dimensional metamaterials of giant chirality[4–6,16,17], the mixing of electric and magnetic responses for oblique incidences to anisotropic metasurfaces[21–23], and 2-dimensional meta-films using the overlap of electric- and magnetic- dipoles[7,8,18] or non-Hermitian electric dipoles[24].

In the context of the achievement of optical SAM, chiral materials alone do not establish the sufficient condition, in spite of their spin-dependent wavevectors (Fig. 1a). This is due to the spin-independent wave impedance of chiral materials, which leads to equal SAM scattering intensity[2,3]; in contrast to gyrotropic materials with spin-dependent *wavevectors and impedances*[3,25]. An alternative route toward optical SAM in the absence of gyrotropic impedance can be made using circular dichroism[2,3,7,8,18,24,26,27] to selectively '*annihilate*' spins (Fig. 1b), yet at the expense of inherent dissipation and the consequent degradation of the quality factor in the system. To achieve *conservative* and high-Q response in optical SAM with nonmagnetic materials, the spectral '*separation*' of spin can be envisaged (as in Fig. 1c), yet has not been sought or demonstrated.

In this paper, we propose and demonstrate the nonmagnetic conservative '*separation*' of optical SAM, derived from the difference of two antisymmetric and spectrally separated Fano resonance spectra (Fig. 1c). Understanding that Fano resonances involve inherently asymmetric spectral profiles with shifted resonances[28–31], it will be shown that, upon the opposite shift of Fano spectral pole for different handedness of photon, the spectral separation of spin and consequently the nonzero value of SAM can be achieved. As an implementation platform, we analyze a chiral resonator with a pair of highly-birefringent mirrors, which provide x- and y- polarization dependent scattering pathways for the Fano interference.

Photonic Systems Laboratory, School of EECS, Seoul National University, Seoul 151-744, Korea. Correspondence and requests for materials should be addressed to N.P. (email: nkpark@snu.ac.kr)

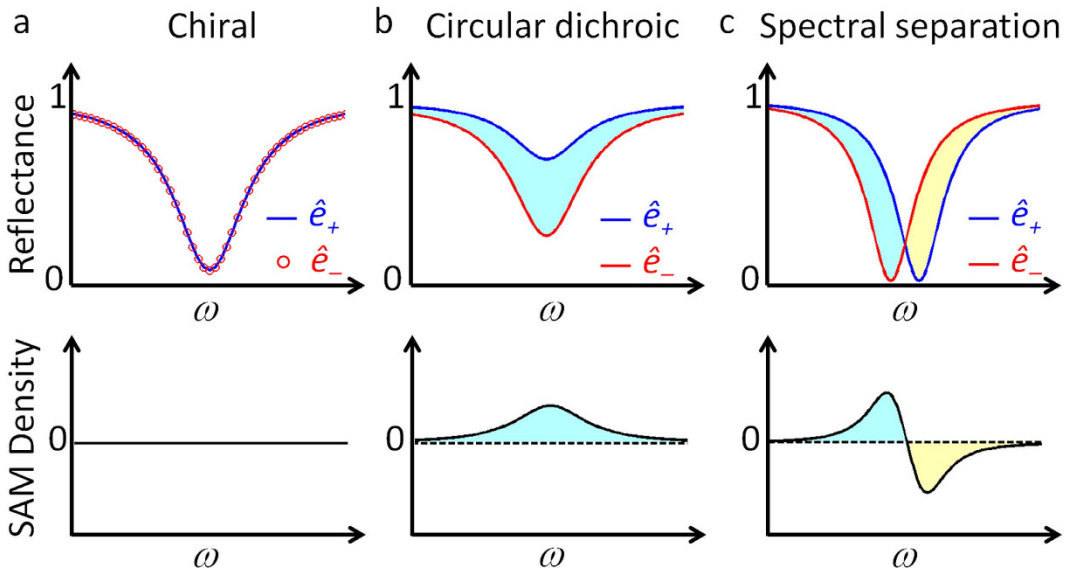

Figure 1. A schematic of reflection spectra for linear polarization and corresponding density of optical SAM; from (a) chiral material, (b) circular dichroic material, and (c) spin-dependent spectral separation system. $\hat{e}_+$ (blue) and $\hat{e}_-$ (red) represent SAM of $+1$ and -1.

By developing a temporal coupled mode theory (CMT)[32,33] for the Fano chiral resonator, we then prove that the handedness of the spin eigenvector is projected onto the temporal domain as an opposite temporal shift, thereby leading to an antisymmetric Fano response in the spectral domain. The spin-density Fano parameter in relation to the material chirality and mirror birefringence is also derived for the quantitative control of optical SAM. Finally, as an application, we propose 'optical spin switching' and the practical design based on indefinite metamaterial mirrors, with experimentally accessible material parameters.

Results

Realization of spin-dependent Fano resonances. Figure 2a shows a schematic diagram of the proposed structure for the Fano-resonant separation of optical SAM. A Fabry-Perot resonator is constructed with a chiral material sandwiched between a pair of birefringent (ε_x, ε_y) mirrors. To clearly isolate the physics of Fano-induced optical SAM from circular dichroism, for the moment we use dielectric constants of real values (inclusion of material loss will be treated later, and also in Supplementary Note 1 and 2). For the special case with isotropic mirrors of $\varepsilon_x = \varepsilon_y$, the response of the resonator per the incidence of x-polarized plane wave is calculated with CMT (see refs 29,30 and Eqs. (1–3) for the spin-form CMT) and a scattering matrix[34], as shown in Fig. 2b,c (with $\varepsilon_{x,y} = \varepsilon_{metal} = -80$ and $\varepsilon_{x,y} = \varepsilon_{dielec} = 2.25$ respectively. please see Supplementary Notes 1 and 2 for its realization). With perfect overlap between the reflection spectra of the $\hat{e}_\pm$ spin modes, there is no optical SAM when $\varepsilon_x = \varepsilon_y$, as expected in refs 2,3.

For comparison, Fig. 2d shows the reflection spectra of the resonator, with the highly *birefringent* film ($\varepsilon_x = \varepsilon_{metal} \ll 0 < \varepsilon_y = \varepsilon_{dielec}$). In stark contrast to the case of $\varepsilon_x = \varepsilon_y$, the spectral separation of the $\hat{e}_\pm$ spin mode ($\hat{e}_+$ in blue and $\hat{e}_-$ in red) and the separation of optical SAM (light-blue and yellow regions, Fig. 2d) is evident. Figure 2e shows the calculated spin density $\sigma = (R_{\hat{e}-} - R_{\hat{e}+})/(R_{\hat{e}-} + R_{\hat{e}+})$, where $R_{\hat{e}\pm}$ is the reflectance of the $\hat{e}_\pm$ component, and $\sigma = \pm 1$ represents the pure spin state $\hat{e}_\pm$. Compared with the case of circular dichroism ($\sigma \sim 0.5$)[27], a much larger spin density value $\sigma \sim 0.998$, close to the pure spin state, is achieved from the difference of two narrowband and antisymmetric Fano profiles. Meanwhile, it is clear that the emergence of Fano resonances for each spin state $\sigma = \pm 1$ is the result of the mixing between the narrowband (Fig. 2b, through x-axis in mirrors) and broadband (Fig. 2c, through y-axis in mirrors) scattering pathways ($\varepsilon_x = \varepsilon_{metal} \ll 0 < \varepsilon_y = \varepsilon_{dielec}$); the underlying physics of the opposite, antisymmetric shift of the Fano spectral pole in relation to the handedness of the spin needs to be further elaborated, as detailed in the later section (see Supplementary Note 3 for the dependency on the state of linear polarizations).

To investigate the origin of the observed spin-dependent antisymmetric Fano responses, we first need to develop a temporal CMT for chiral resonances. Considering the natural optical rotation 2θ ($\theta = \omega\chi L_{eff}/2c$, χ: normalized chirality, L_{eff}: effective path, c: speed of light)[2,3] inside the resonator, we introduce the 'rotated' coordinates (h- and v-axes in Fig. 3a) for a chiral medium. The chiral resonant mode can then be decomposed into two linear resonant modes (a_h, a_v), orthogonal to each other and having modal decay times of τ_h and τ_v respectively (Fig. 3a). Because the h- and v-axes are rotated by θ from the middle of the cavity to the mirror, we obtain $1/\tau_h = \cos^2\theta/\tau_x + \sin^2\theta/\tau_y$ and $1/\tau_v = \sin^2\theta/\tau_x + \cos^2\theta/\tau_y$, where τ_x and τ_y are the

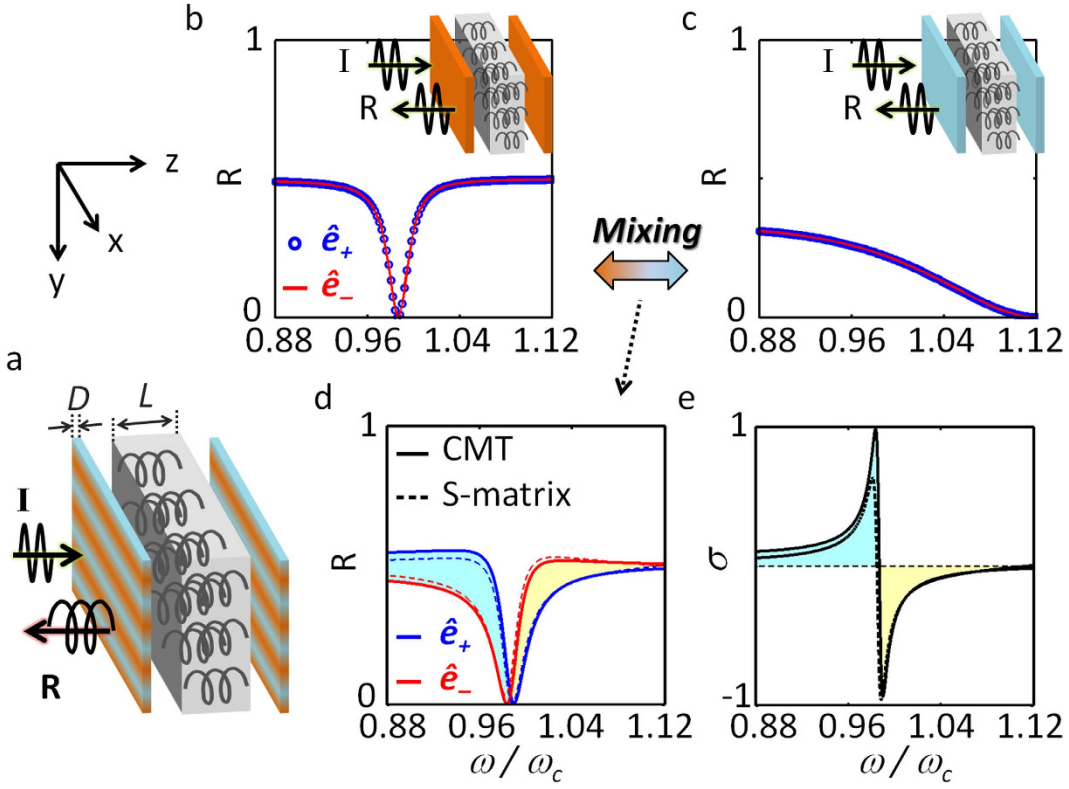

Figure 2. Spectral separation of optical SAM based on antisymmetric Fano resonances. (**a**) Proposed chiral resonator for SAM separation. A layer of a chiral medium ($L = 0.29\lambda_c$ where $\lambda_c = 2\pi c/\omega_c$ and ω_c is the normalization frequency, $\varepsilon_{chiral} = 9$, $\chi = 0.05$) is enclosed by a pair of birefringent mirrors ($\varepsilon_x = \varepsilon_{metal} = -80$, $\varepsilon_y = \varepsilon_{dielec} = 2.25$, $D = \lambda_c/60$). Reflection spectra of $\hat{e}_+$ (blue) and $\hat{e}_-$ (red) spin modes with (**b**) metallic mirrors ($\varepsilon_x = \varepsilon_y = \varepsilon_{metal}$), (**c**) dielectric mirrors ($\varepsilon_x = \varepsilon_y = \varepsilon_{dielec}$), and (**d**) highly-birefringent mirrors ($\varepsilon_x = \varepsilon_{metal}$, $\varepsilon_y = \varepsilon_{dielec}$). (**e**) Spectra of SAM density σ (± 1 denotes pure $\hat{e}_\pm$) with birefringent mirrors. The calculations are based on both CMT (solid) and a scattering matrix (dashed). The CMT fitting values for the resonance ($\omega_x = 0.987\omega_c$ and $\omega_y = 0.571\omega_c$) and Q-factors ($Q_x = 100$ and $Q_y = 12$) for each mode (Fig. 2b,c) were obtained from the scattering matrix results.

decay times for each birefringence axis ($\tau_x \neq \tau_y$ when $\varepsilon_x \neq \varepsilon_y$). The CMT equation in h- and v- coordinates then becomes

$$\frac{d}{dt}\begin{bmatrix} a_h \\ a_v \end{bmatrix} = \begin{bmatrix} i\omega_{h0} - 2/\tau_h & 0 \\ 0 & i\omega_{v0} - 2/\tau_v \end{bmatrix} \cdot \begin{bmatrix} a_h \\ a_v \end{bmatrix}, \tag{1}$$

where ω_{h0} (or ω_{v0}) is the resonant frequency of the a_h (or a_v) mode. Upon the incident of x- and y-polarized waves (S_{1x+}, S_{1y+}) to the resonator (Fig. 3b), their couplings to resonance modes (a_h, a_v) are thus written as

$$\frac{d}{dt}\begin{bmatrix} a_h \\ a_v \end{bmatrix} = \begin{bmatrix} i\omega_{h0} - 2/\tau_h & 0 \\ 0 & i\omega_{v0} - 2/\tau_v \end{bmatrix} \begin{bmatrix} a_h \\ a_v \end{bmatrix} + \begin{bmatrix} \kappa_h & 0 \\ 0 & \kappa_v \end{bmatrix} U_r \begin{bmatrix} {S_{1x}}^{in} \\ {S_{1y}}^{in} \end{bmatrix}, \tag{2}$$

where U_r is the rotation matrix of $[\cos\theta, \sin\theta; -\sin\theta, \cos\theta]$ and $\kappa_{h,v} = (2/\tau_{h,v})^{1/2}$ is the excitation coupling coefficient to the resonator[32,33].

In terms of the optical SAM, it is convenient to use a spin-basis representation of Eq. (2). Taking the spin form of $a_\pm = a_h \mp i a_v$ and ${S_{1\pm}}^{in} = {S_{1x}}^{in} \mp {S_{1y}}^{in}$, we then achieve the spin-form CMT, upon the incident wave of $\boldsymbol{S}_{in} = [{S_{1+}}^{in}; {S_{1-}}^{in}]$ as follows:

$$\frac{d}{dt}\begin{bmatrix} a_+ \\ a_- \end{bmatrix} = i\begin{bmatrix} \omega_s & \omega_d \\ \omega_d & \omega_s \end{bmatrix}\begin{bmatrix} a_+ \\ a_- \end{bmatrix} + \begin{bmatrix} \kappa_s e^{-i\theta} & \kappa_d e^{i\theta} \\ \kappa_d e^{-i\theta} & \kappa_s e^{i\theta} \end{bmatrix}\overrightarrow{S_{in}}, \tag{3}$$

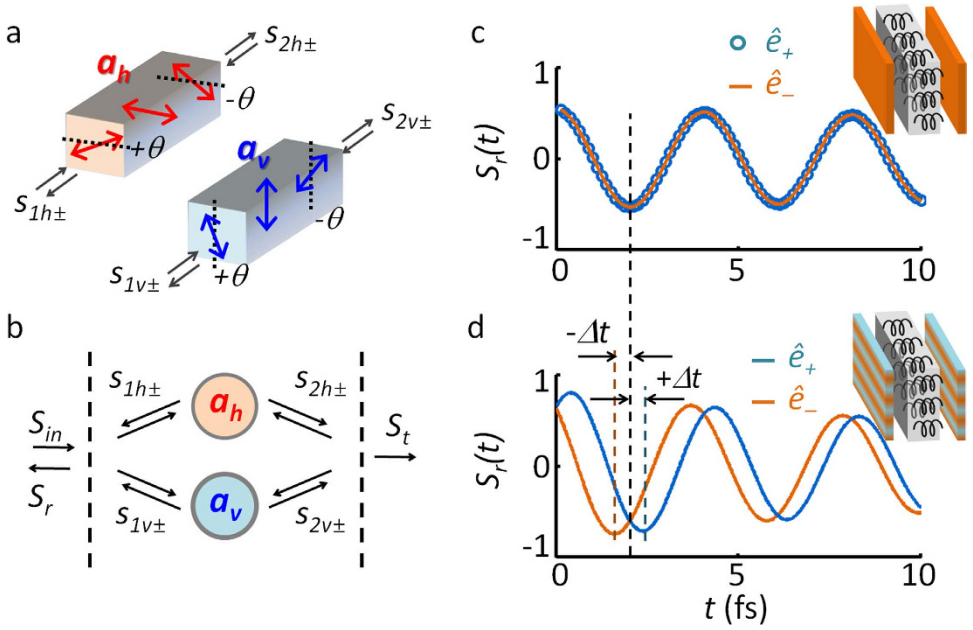

Figure 3. Coupled mode analysis for Fano-chiral systems. (**a**) Representation of a chiral resonator in linear basis h and v, including natural optical rotation (horizontal and vertical in the middle of the resonator and rotated by $\pm\theta$ at the two interfaces). $S_{1(2)h(v)\pm}$ denotes the respective polarization component of incident wave at the interface. (**b**) The CMT model of the chiral resonator illustrated in Fig. 2a, with S_{in}: incidence, S_r: reflection, and S_t: transmission. (**c**,**d**) Impulse responses of the resonator for different spins ($S_{1x}^{in} = \delta(t)$, $\hat{e}_+$: blue, $\hat{e}_-$: red), with (**c**) $\varepsilon_x = \varepsilon_y = \varepsilon_{metal}$ and (**d**) $\varepsilon_x = \varepsilon_{metal}$, $\varepsilon_y = \varepsilon_{dielec}$. The dashed lines indicate temporal shifts of $\Delta t = 2\theta/\omega_c$, obtained for $\hat{e}_\pm$ respectively. All of the results are calculated using the temporal CMT equation (Eq. (3)).

where $\omega_s = (\omega_{h0} + \omega_{v0})/2 + i\cdot(1/\tau_h + 1/\tau_v)$, $\omega_d = (\omega_{h0} - \omega_{v0})/2 + i\cdot(1/\tau_h - 1/\tau_v)$, $\kappa_s = (\kappa_h + \kappa_v)/2$, and $\kappa_d = (\kappa_h - \kappa_v)/2$. We emphasize that this spin-form CMT (Eq. (3)) clearly reveals the underlying physics of the spin-dependent Fano responses. First, mixing between spin modes a_+ and a_- through nonzero ω_d and κ_d arises when $\tau_x \neq \tau_y$ (the birefringent mirror case), breaking the spectral degeneracy of the spin modes. Second, the incident waves undergo phase evolutions through $\kappa_s e^{\pm i\theta}$, in *opposite* directions for $\hat{e}_+$ and $\hat{e}_-$ spins, thus deriving the antisymmetric Fano response for opposite spins.

The temporal interpretation of Fano dynamics[35], for the impulse response of Eq. (3) with $S_{1x}^{in} = \delta(t)$, further elucidates the origin of antisymmetric Fano resonances for opposite spin states. Figure 3c,d show the impulse responses of the chiral resonators, having isotropic and birefringence mirrors respectively. The temporal phase shift corresponding to Fano resonance[35], especially in the opposite direction for the $\hat{e}_+$ and $\hat{e}_-$ spin modes, exposes only when both conditions of $\theta \neq 0$ (chiral medium) and $\tau_h \neq \tau_v$ (birefringent mirrors) are met at the same time. In detail, the phase shift for each spin $\hat{e}_+$ and $\hat{e}_-$ takes the form of time-leading and lagging ($\Delta t = 2\theta/\omega_c$), from the different scattering paths $\kappa_d e^{\pm i\theta}$ (Eq. (3)). In the spectral representation these temporal shifts correspond to shifts in the Fano resonant poles[35] in opposite directions, and thus lead to two antisymmetric and spectrally separated Fano resonance spectra (Fig. 2d).

Control of Fano resonances for optical spin switching. Upon revealing the physics behind the Fano-induced optical SAM, we now examine the key parameters for its control in detail. To quantitatively assess the behavior of the system, by following the definition of the Fano parameter[28] here we define a spin-density Fano parameter q_s ; as the ratio of indirect- to direct-excitation of the resonator, in this case $\kappa_d e^{i\theta}$ and $\kappa_s e^{-i\theta}$ (Eq. (3)). Then, we obtain

$$q_s = \frac{\kappa_d}{\kappa_s} e^{i2\theta}. \tag{4}$$

Figure 4 presents the spin-density spectra as a function of the argument $arg(q_s) = 2\theta$ (chirality) and modulus $|q_s| = \kappa_d/\kappa_s$ (birefringence) of the Fano parameter. As observed in Fig. 4a, the bandwidth of the spin density σ decreases for smaller $arg(q_s) = 2\theta$, which is associated with the smaller spectral separations between the $\hat{e}_+$ and $\hat{e}_-$ modes (as in Fig. 4b). The spin-density spectra for different $|q_s|$ is also plotted in Fig. 4c, showing a smaller bandwidth for larger $|q_s|$, which is again associated with the decrease in the spectral separation between the $\hat{e}_+$ and $\hat{e}_-$ modes (Fig. 4d).

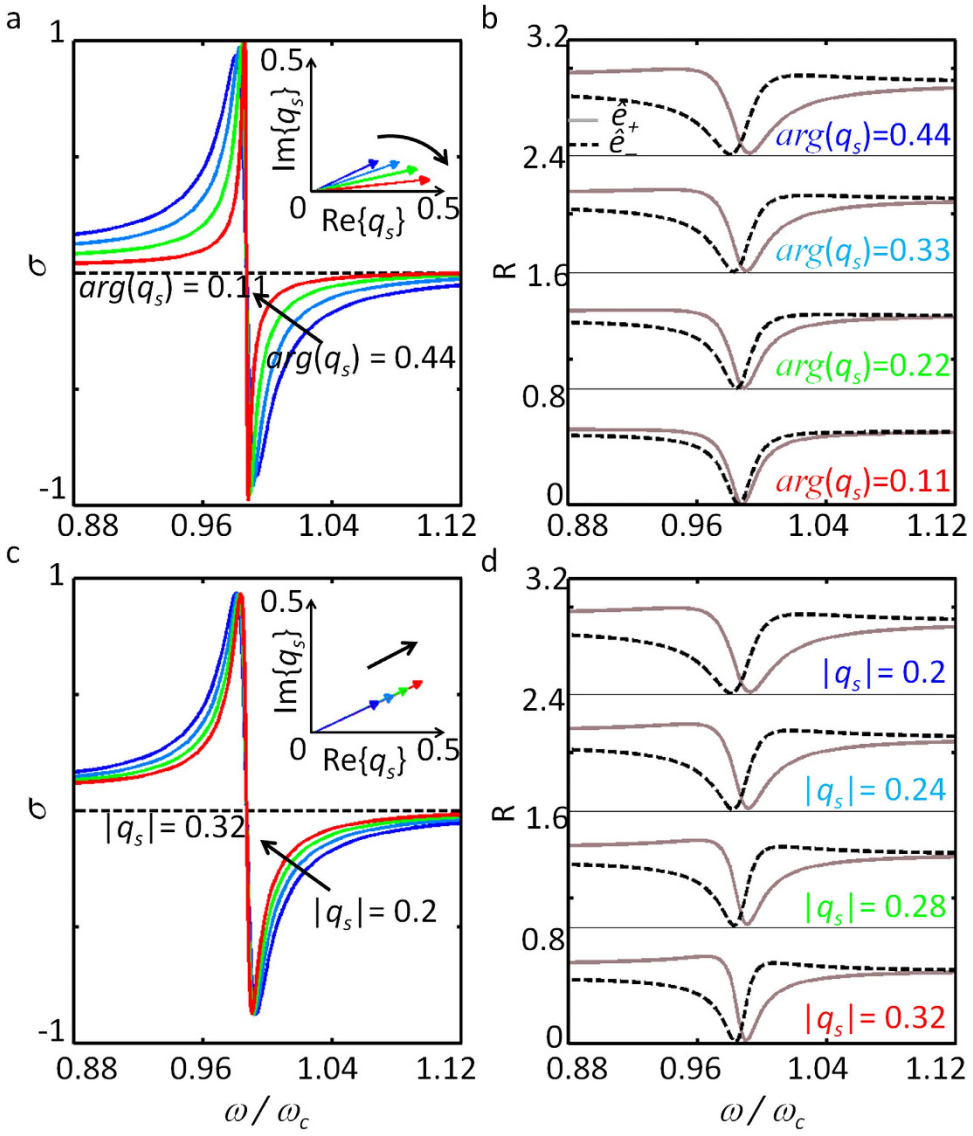

Figure 4. Optical spin-density and reflection spectra as a function of (a,b) chirality i.e. $arg(q_s) = 0.44$ to 0.11 and (c,d) birefringence i.e. $|q_s| = 0.2$ to 0.32. In (**b**,**d**) the $\hat{e}_+$ (solid) and $\hat{e}_-$ (dashed) lines represent the states of spin-density $\sigma = +1$ and -1, respectively.

Utilizing the sharp transition of the σ, reversing its sign from $+1$ to -1 within $\Delta\omega \sim \omega_c/250$ (Fig. 4), we demonstrate '*optical spin switching*', for the first time to our knowledge. Here we assume spin switching based on the control of $arg(q_s)$, or equivalently $\chi \cdot L_{\text{eff}}$. Figure 5a shows the schematics of the suggested device, which has two electrodes connected to the chiral medium for the control of L_{eff} via refractive index tuning (e.g., $\Delta n \sim 0.008$ can be achieved with an ~1 V bias voltage[36–38]). For the change of $\Delta n = 10^{-3}$, in Fig. 5b we show the consequent shift of the spin density spectra, which derives a sharp transition in σ ; from $\sigma = +0.998$ (bias off, blue) to $\sigma = -0.993$ (bias on, red) at the working frequency $\omega = 0.987\omega_c$ and chirality $\chi = 0.005$. As shown in Fig. 5c, even smaller values of χ ($=10^{-1}$ to 10^{-4}) and smaller tuning of Δn (10^{-2} to 10^{-5}) for spin switching is also possible, but at the expense of a reduction in reflectance (0.4 to 10^{-4}, Fig. 5d). To achieve larger signal strength, chiral metamaterials of lager χ ($\chi \sim 1$)[4–6,27] combined with background materials with larger index tuning ($\Delta n > 10^{-3}$, such as liquid crystals) could be used with a minor penalty in the purity of the spin. The effect of material loss is also investigated (Fig. 5e,f), by introducing complex-valued resonant frequencies (as in refs 32,33), of ω_{h0} and ω_{v0} in Eq. (2): in terms of intrinsic quality factor of each resonant mode $Q_{int} = Re[\omega_{h,v0}]/(2 \cdot Im[\omega_{h,v0}])$. Due to the spectral broadening and imperfect critical coupling from material loss, the purity of the spin density decreases (Fig. 5e), yet with the overall increase in its reflectance (Fig. 5f).

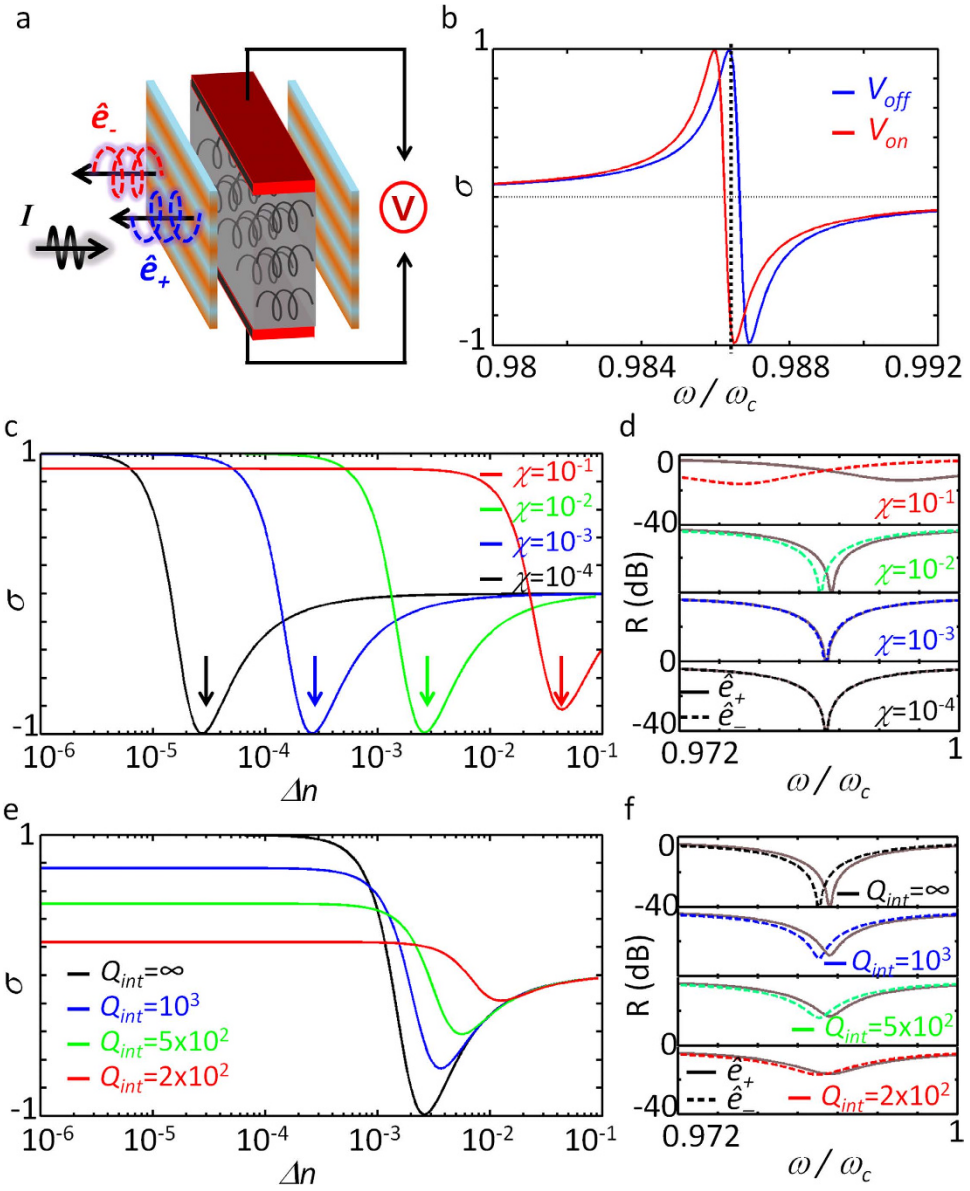

Figure 5. Optical spin switching based on Fano resonances. (**a**) Schematics of the optical spin switching. (**b**) Spin-density spectra without (blue, V_{off}) and with electric bias (red, V_{on}, $\Delta n = 0.001$). At the frequency $0.987\omega_c$, spin reversal from $\sigma = +0.998$ (blue) to $\sigma = -0.993$ (red) is observed. All of the geometrical parameters are the same as those in Fig. 2a, except for $\chi = 0.005$. (**c**) The spin density as a function of chirality χ (10^{-1} to 10^{-4}) and applied Δn (10^{-6} to 10^{-1}). The magnitude of Δn_R required for the spin reversal for each value of χ is marked with arrows. (**d**) Reflectance spectra for $\hat{e}_+$ (solid lines) and $\hat{e}_-$ (dashed lines) at each value of χ and Δn_R. The effect of material loss for optical spin switching is also presented in terms of (**e**) the spin density and (**f**) reflectance spectra: for different values of intrinsic quality factor of each resonant mode $Q_{int} = 2 \times 10^2$ to 10^3. $\chi = 10^{-2}$.

Discussion

In this work, we propose a new pathway for the nonmagnetic achievement of optical spin angular momentum based on the spin-dependent separation of Fano resonance spectra. By developing a spin-form temporal CMT for the chiral resonator, we unveil the origin of the spin-dependent antisymmetric Fano resonance in perfect agreement with the scattering matrix calculations. A spin-density Fano parameter is derived to identify key parameters for quantitative control of the optical SAM in the spectral domain. Based on the spectrally-sensitive characteristics of the Fano resonance, 'optical spin switching' is proposed for the first time, with experimentally accessible parameter values. From an order of magnitude reduction of material chirality required for optical SAM generation (Fig. 5c–f), we can also envisage the applications for bio-chemical sensing: the sensing of organic helical structures (very weak chirality from the displacement current) without any metallic inclusions (strong chirality from the conduction

current). In Supplementary Information, we provided the real implementation of Fano- induced spectral separation of optical SAM using highly-birefringent mirrors (Supplementary Note 1, see Supplementary Fig. 2 for their fabrication process), especially analyzing the property of birefringent mirrors in IR and THz regimes (Supplementary Note 2). Our results, which are based on 'conservative (lossless)' optical elements fundamentally distinctive from non-conservative circular dichroism, not only derive high-Q responses from the Hermiticity, but also allow excellent purity in spin density ($P_{RCP}/P_{LCP} < -15$ dB in Figs 2 and 4, with practical parameters both in IR and THz regimes) comparable to the previous record in circular dichroism ($P_{RCP}/P_{LCP} = -1.5$ dB in the IR range[39], and -25 dB in the microwave range[40]).

References

1. Van Enk, S. & Nienhuis, G. Spin and orbital angular momentum of photons. *Europhys. Lett.* **25,** 497 (1994).
2. Serdyukov, A., Semchenko, I., Tretyakov, S. & Sihvola, A. *Electromagnetics of bi-anisotropic materials: Theory and applications*. (Gordon and Breach Science, 2001).
3. Orfanidis, S. J. *Electromagnetic waves and antennas*. (Rutgers University New Brunswick, NJ, 2002).
4. Gansel, J. K. *et al.* Gold helix photonic metamaterial as broadband circular polarizer. *Science* **325,** 1513–1515 (2009).
5. Thiel, M., Rill, M. S., von Freymann, G. & Wegener, M. Three-Dimensional Bi-Chiral Photonic Crystals. *Advanced Materials* **21,** 4680–4682 (2009).
6. Zhao, Y., Belkin, M. & Alù, A. Twisted optical metamaterials for planarized ultrathin broadband circular polarizers. *Nature Comm.* **3,** 870 (2012).
7. Fedotov, V. *et al.* Asymmetric propagation of electromagnetic waves through a planar chiral structure. *Phys. Rev. Lett.* **97,** 167401 (2006).
8. Li, Z., Gokkavas, M. & Ozbay, E. Manipulation of asymmetric transmission in planar chiral nanostructures by anisotropic loss. *Advanced Optical Materials* **1,** 482–488 (2013).
9. Chen, S. *et al.* Circularly polarized light generated by photoexcitation of luminophores in glassy liquid-crystal films. *Nature* **397,** 506–508 (1999).
10. Furumi, S. & Tamaoki, N. Glass-Forming Cholesteric Liquid Crystal Oligomers for New Tunable Solid-State Laser. *Advanced Materials* **22,** 886–891 (2010).
11. Saenz, E. *et al.* Modeling of spirals with equal dielectric, magnetic, and chiral susceptibilities. *Electromagnetics* **28,** 476–493 (2008).
12. Tang, Y. & Cohen, A. E. Optical chirality and its interaction with matter. *Phys. Rev. Lett.* **104,** 163901 (2010).
13. Tang, Y. & Cohen, A. E. Enhanced enantioselectivity in excitation of chiral molecules by superchiral light. *Science* **332,** 333–336 (2011).
14. Brasselet, E. *et al.* Dynamics of optical spin-orbit coupling in uniaxial crystals. *Opt. Lett.* **34,** 1021–1023 (2009).
15. Asenjo-Garcia, A. & de Abajo, F. G. Dichroism in the Interaction between Vortex Electron Beams, Plasmons, and Molecules. *Phys. Rev. Lett.* **113,** 066102 (2014).
16. Pendry, J. B. A chiral route to negative refraction. *Science* **306,** 1353–1355, doi: 10.1126/science.1104467 (2004).
17. Zhang, S. *et al.* Negative refractive index in chiral metamaterials. *Phys. Rev. Lett.* **102,** 023901 (2009).
18. Plum, E. *et al.* Metamaterial with negative index due to chirality. *Phys. Rev. B* **79,** 035407 (2009).
19. Khanikaev, A. B. *et al.* Photonic topological insulators. *Nature Mater.* **12,** 233–239 (2013).
20. Rechtsman, M. C. *et al.* Photonic Floquet topological insulators. *Nature* **496,** 196–200 (2013).
21. Hao, J. *et al.* Manipulating electromagnetic wave polarizations by anisotropic metamaterials. *Phys. Rev. Lett.* **99,** 063908 (2007).
22. Pu, M. *et al.* Anisotropic meta-mirror for achromatic electromagnetic polarization manipulation. *Appl. Phys. Lett.* **102,** 131906 (2013).
23. Plum, E. *et al.* Metamaterials: optical activity without chirality. *Phys. Rev. Lett.* **102,** 113902 (2009).
24. Yu, S., Park, H. S., Piao, X., Min, B. & Park, N. Chiral interactions of light induced by low-dimensional dynamics in complex potentials. *arXiv preprint arXiv:1409.0180* (2014).
25. Martin, D., Neal, K. & Dean, T. The optical and magneto-optical behaviour of ferromagnetic metals. *Proceedings of the Physical Society* **86,** 605 (1965).
26. Cao, T. *et al.* Valley-selective circular dichroism of monolayer molybdenum disulphide. *Nature Comm.* **3,** 887 (2012).
27. Droulias, S. & Yannopapas, V. Broad-band giant circular dichroism in metamaterials of twisted chains of metallic nanoparticles. *The Journal of Physical Chemistry C* **117,** 1130–1135 (2013).
28. Fano, U. Effects of configuration interaction on intensities and phase shifts. *Phys. Rev.* **124,** 1866 (1961).
29. Luk'yanchuk, B. *et al.* The Fano resonance in plasmonic nanostructures and metamaterials. *Nature Mater.* **9,** 707–715 (2010).
30. Piao, X., Yu, S., Koo, S., Lee, K. & Park, N. Fano-type spectral asymmetry and its control for plasmonic metal-insulator-metal stub structures. *Opt. Express* **19,** 10907–10912 (2011).
31. Piao, X., Yu, S. & Park, N. Control of Fano asymmetry in plasmon induced transparency and its application to plasmonic waveguide modulator. *Opt. Express* **20,** 18994–18999 (2012).
32. Haus, H. A. *Waves and fields in optoelectronics*. Vol. 464 (Prentice-Hall Englewood Cliffs, NJ, 1984).
33. Joannopoulos, J. D., Johnson, S. G., Winn, J. N. & Meade, R. D. *Photonic crystals: molding the flow of light*. (Princeton university press, 2011).
34. Tikhodeev, S. G., Yablonskii, A. L., Muljarov, E. A., Gippius, N. A. & Ishihara, T. Quasiguided modes and optical properties of photonic crystal slabs. *Phys. Rev. B* **66,** doi: 10.1103/PhysRevB.66.045102 (2002).
35. Ott, C. *et al.* Lorentz meets Fano in spectral line shapes: a universal phase and its laser control. *Science* **340,** 716–720 (2013).
36. Dionne, J. A., Diest, K., Sweatlock, L. A. & Atwater, H. A. PlasMOStor: a metal− oxide− Si field effect plasmonic modulator. *Nano Lett.* **9,** 897–902 (2009).
37. Lee, H. W. *et al.* Nanoscale Conducting Oxide PlasMOStor. *Nano Lett.* **14,** 6463–6468 (2014).
38. Aitchison, J., Hutchings, D., Kang, J., Stegeman, G. & Villeneuve, A. The nonlinear optical properties of AlGaAs at the half band gap. *Quantum Electronics, IEEE Journal of* **33,** 341–348 (1997).
39. Cui, Y., Kang, L., Lan, S., Rodrigues, S. & Cai, W. Giant chiral optical response from a twisted-arc metamaterial. *Nano Lett.* **14,** 1021–1025 (2014).
40. Ma, X. *et al.* Multi-band circular polarizer using planar spiral metamaterial structure. *Opt. Express* **20,** 16050–16058 (2012).

Acknowledgements

This work was supported by the National Research Foundation of Korea through the Global Frontier Program (GFP) NRF-2014M3A6B3063708, and the Global Research Laboratory (GRL) Program

K20815000003, which are all funded by the Ministry of Science, ICT & Future Planning of the Korean government.

Author Contributions

X.P. and N.P. conceived of the presented idea. X.P. developed the theory and performed the computations. S.Y. and J.H. verified the analytical methods. N.P. encouraged X.P. to investigate Fano resonances and supervised the findings of this work. All authors discussed the results and contributed to the final manuscript.

Additional Information

Supplementary information accompanies this paper at http://www.nature.com/srep

Competing financial interests: The authors declare no competing financial interests.

How to cite this article: Piao, X. *et al.* Spectral separation of optical spin based on antisymmetric Fano resonances. *Sci. Rep.* **5**, 16585; doi: 10.1038/srep16585 (2015).